TECTONICS, VOL. 15, NO. 2, PAGES, 387-402, APRIL 1996

Listric normal faulting during postorogenic extension revealed by $^{40}Ar/^{39}Ar$ thermochronology near the Robertson Lake shear zone, Grenville orogen, Canada

Jay P. Busch, Ben A. van der Pluijm, Chris M. Hall, and Eric J. Essene
Department of Geological Sciences, University of Michigan, Ann Arbor

Abstract. The Robertson Lake shear zone is a major plastic to brittle extensional shear zone in the Grenville orogen that bounds the Mazinaw and Sharbot Lake domains and provides information on the style of late extension and the unroofing history of the orogen. Argon isotope data were collected from hornblende and micas to determine $^{40}Ar/^{39}Ar$ ages, constrain the temperature-time histories of these two domains, and infer the unroofing history of the region. Hornblende cooling ages across the Mazinaw domain (footwall) show little variation, indicating uniform unroofing of the footwall since 950 Ma. Phlogopite, muscovite, and biotite cooling ages of the footwall are 924 to 890 Ma. The cooling history of the Mazinaw domain is characterized by slow cooling after peak metamorphism (circa 1000 Ma), accelerated cooling (4°-5°C/m.y.) from 950 Ma to 890 Ma, and an average cooling rate of ~1°C/m.y. to circa 590 Ma, when these rocks were at or near the surface. The cooling history of Sharbot Lake (hanging wall) domain is drastically different than that of the Mazinaw domain. Hornblende and biotite cooling ages in the central portion of the domain are 1009 and 969 Ma, respectively, indicating a cooling rate of 5°C/m.y. after slow cooling from metamorphic temperatures. Biotite and phlogopite cooling ages determined from samples located at different distances from the shear zone do not lie along the same cooling curve, indicating that the cooling history varied across the domain. Cooling rates in the hanging wall adjacent to the shear zone are low (2°C/m.y.). A biotite cooling age (1029 Ma) and preservation of an amphibole growth age (1205 Ma) in the hanging wall adjacent to the shear zone reflect shallow crustal levels for this sample since 1205 Ma. These data indicate that the hanging wall away from the shear zone was unroofed from deeper crustal levels faster and much later than the hanging wall adjacent to the shear zone. The varied cooling histories across the region are resolved by listric normal faulting that lead to uniform unroofing of the footwall and differential unroofing across the hanging wall due to rotation during fault displacement.

Introduction

The Grenville Province of southeastern Ontario, Canada is considered to be the root of a Middle Proterozoic mountain belt that is composed of deformed and metamorphosed middle to lower crustal rocks [e.g., *Dewey and Burke*, 1973; *Windley*, 1986]. The structures in these rocks have traditionally been interpreted to be a product of the amalgamation of terranes in a series of contraction dominated orogenic events [*Davidson*, 1984; *Hanmer*, 1988; *Rivers et al.*, 1989; *Easton*, 1992; *White et al.*, 1994; *Zelt et al.*, 1994]. In recent years the significance of extensional deformation in this orogen has become evident [*van der Pluijm and Carlson*, 1989; *Cosca et al.*, 1991, 1992, 1995; *Mezger et al.*, 1991; *Culshaw et al.*, 1994; *Busch and van der Pluijm*, 1995]. The timing and style of extension associated with individual shear zones are important for evaluating the role of extension in orogenesis. This information, when combined with data regarding timing and style of magmatism, relative timing of compression and extension, and overall orogenic structure, may ultimately provide evidence for the mechanisms of extension [e.g., *Dewey*, 1988; *Platt and England*, 1994]. Extensional displacement along shear zones during or after cooling from metamorphic temperatures has resulted in varied cooling histories across the Metasedimentary Belt [*Cosca et al.*, 1992]. Cooling histories can be used to test aspects of tectonic and structural models that cannot be derived from metamorphic and structural studies alone [e.g., *van der Pluijm et al.*, 1994; *Cosca et al.*, 1995; *Fillipone et al.*, 1995; *Lee*, 1995]. This approach is particularly applicable to the late tectonic history (postorogenic) during and after cooling from peak metamorphic temperatures.

Easton [1988a] documented the significance of the Robertson Lake shear zone (RLSZ), which separates two domains in the southeastern Metasedimentary Belt (Figure 1). *Cosca et al.* [1991] found a 70 m.y. difference in hornblende $^{40}Ar/^{39}Ar$ cooling ages between the Mazinaw and Sharbot Lake domains, which was attributed to differential unroofing due to extensional deformation along the RLSZ. Based on hornblende cooling ages, the regional thermochronologic study by *Cosca et al.* [1992] constrained the timing of extension along the RLSZ to at least 934 Ma. However, these inferences were based only on hornblende $^{40}Ar/^{39}Ar$ analyses, with just one sample located in the Sharbot Lake domain. Structural observations and two $^{40}Ar/^{39}Ar$ analyses of biotite have corroborated the interpretation of late extensional deformation and further constrained the timing of extensional displacement until at least 900 Ma [*Busch and van der Pluijm*, 1995]. The purpose of this study is to define the cooling histories of the Mazinaw and Sharbot Lake domains by $^{40}Ar/^{39}Ar$ analyses of hornblendes and micas in both domains. These data provide constraints on the unroofing history adjacent to the RLSZ. In addition, local variations in cooling history provide information on the style of late orogenic extension in these rocks.

Paper number 95TC03501.
0278-7407/96/95TC-03501$10.00

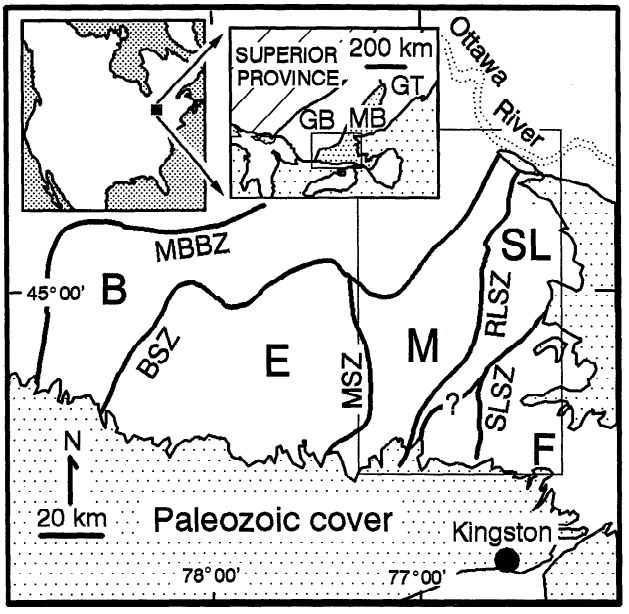

Figure 1. General subdivision of the Metasedimentary Belt (modified from *Easton* [1992]). Abbreviations are B, Bancroft domain; E, Elzevir domain; M, Mazinaw domain; SL, Sharbot Lake domain; F, Frontenac domain; MBBZ, Metasedimentary Belt boundary zone; BSZ, Bancroft shear zone; MSZ, Mooroton shear zone; RLSZ, Robertson Lake shear zone; SLSZ, Sharbot Lake shear zone. Boundary with a question mark indicates a possible Mazinaw-Sharbot Lake boundary inferred by *Easton* [1992]. Light stipple is Paleozoic cover. Insets show location of study area relative to North America and major subdivisions of the Grenville orogen in Canada. Other abbreviations are GB, Granulite Belt; MB, Metasedimentary Belt; GT, Granulite Terrane. Box outlines area of Figure 3.

Regional Geology

The Metasedimentary Belt is composed of marble, clastic metasedimentary rocks, and a variety of plutonic and volcanic rocks; it has been divided into five lithotectonic domains based on geophysical, lithologic, and chronologic data [*Easton*, 1992]. The RLSZ separates the Sharbot Lake and Mazinaw domains (Figure 1). The term domain is used to describe an assemblage of rocks with distinct lithologic, metamorphic, and geophysical characteristics but does not necessarily imply a genetic distinction. The RLSZ was first recognized by *Smith* [1958], and subsequent work by *Easton* [1988a] identified the regional extent and the contrast in metamorphic facies and lithologies on either side of the zone. The zone has been defined as an east-southeast dipping crystal-plastic mylonite zone with abundant normal shear-sense indicators and locally intense cataclastic deformation [*Jackson*, 1980; *Carter*, 1981; *Easton*, 1988b, c; *Busch and van der Pluijm*, 1995]. A zone of brittle deformation overlies mylonite and contains slip-sense indicators of normal movement along brittle faults of the RLSZ [*Wolff*, 1985; *Pauk*, 1989a, b; *Busch and van der Pluijm*, 1995].

The Mazinaw domain is dominated by deformed granite and tonalite plutons, clastic metasedimentary rocks (quartzofeldspathic schist, gneiss and mica schist), and metavolcanic rocks (amphibole schist) metamorphosed at upper greenschist to upper amphibolite facies conditions with grade increasing from west to east [*Hutcheon and Moore*, 1973; *Sethuraman and Moore*, 1973; *Carmichael et al.*, 1978; *Busch et al.*, 1995]. The oldest igneous rocks of the Mazinaw domain have crystallization ages between 1240 and 1270 Ma [*van Breemen and Davidson*, 1988; *Lumbers et al.*, 1990; *Corfu and Easton*, 1995]. These basement rocks were subsequently unroofed prior to deposition of the Flinton Group metasedimentary rocks, which contain detrital zircons as young as 1150 Ma [*Sager-Kinsman and Parrish*, 1993]. As many as three metamorphic events may have affected these rocks. Accretion of the Metasedimentary Belt to the Gneiss Belt (circa 1190 Ma), collisional reactivation of the Metasedimentary Belt boundary zone (1080 - 1060 Ma), and a later metamorphic event contemporaneous with synorogenic extension (995 - 1050 Ma) have resulted in a complex tectonometamorphic history [*Mezger et al.*, 1991, 1993; *Easton*, 1992; *McEachern and van Breemen*, 1993; *Corfu and Easton*, 1995]. The Mazinaw domain is bounded to the west by the Mooroton shear zone, near vertical mylonite zone [*Cureton*, 1994].

The Sharbot Lake domain is dominated by mafic and intermediate meta-igneous rock and marble. Adjacent to the RLSZ, upper greenschist facies metamorphic conditions are preserved. Marbles are fine grained and preserve bedding near the RLSZ, and some metavolcanic rocks contain primary volcanic features [*Easton*, 1992]. To the east, away from the RLSZ, coarse crystalloblastic garnet-amphibole schists and gneisses are present 15 km northeast of Sharbot Lake. Metamorphic data show an increase in metamorphic grade to near granulite facies conditions to the south and east [*Carmichael et al.*, 1978; *Easton*, 1988c, 1992; *Busch et al.*, 1995]. The oldest igneous crystallization ages in the Sharbot Lake domain from U/Pb zircon dates range from 1254 to 1210 Ma [*Wallach*, 1974; *Corfu and Easton*, 1994]. Younger plutonic rocks yield U/Pb ages of circa 1150 Ma and 1070 Ma [*Corfu et al.*, 1995; A. Davidson, personal communication, 1995]. The youngest metamorphic event dated (U/Pb from zircons and sphenes) in the Sharbot Lake domain is ~1160 Ma [*Mezger et al.*, 1993, *Corfu et al.*, 1995]. The Sharbot Lake domain is bounded to the east by the Sharbot Lake shear zone (also known as the Maberly shear zone), a zone of mylonitic rocks that dip 35°-70° to the east and southeast [*Easton*, 1988c; *Davidson and Ketchum*, 1993].

Analytical Techniques

Electron Microprobe Analyses

Preliminary sample selection for $^{40}Ar/^{39}Ar$ analyses was done using polished thin sections and a standard petrographic microscope. A Cameca Camebax electron microprobe analyzer equipped with a backscattered electron imager at the University of Michigan was used to further characterize the samples and to determine mineral chemistry using wavelength-dispersive analysis. Electron microprobe operating conditions were an accelerating voltage of 15 kV and a sample current of 10 nA except for micas, which were analyzed with a 12 kV accelerating voltage. A mixture of synthetic and natural mineral standards and correction routines of *Pouchou and Pichoir* [1984] (PAP) provided by Cameca was used. A point

beam was used for amphiboles, and the beam was rastered over a 9 μm^2 area to minimize loss of light elements for micas.

The $^{40}Ar/^{39}Ar$ analyses

A laser step-heating technique was used on purified mineral separates [*Meert et al.*, 1994]. Rock samples were crushed, sieved, and separated using standard magnetic separation techniques. Grains were cleaned in deionized water in an ultrasonic bath and pure mineral separates were selected using a binocular microscope. Each sample consisted of 10-20 grains for hornblende and 1-3 grains for micas. Samples were packaged and irradiated at the University of Michigan's Ford Phoenix reactor at location L67 for 90 MWh. Neutron flux gradients were monitored with the MMhb-1 standard using an age of 520.4 Ma [*Samson and Alexander*, 1987]. An argon-ion laser system was used for step heating by defocusing the beam to uniformly heat the grain(s) and increasing the laser power. Each step consisted of heating for 60 seconds followed by 2 minutes of gas purification using two 10 L/s getter pumps (ST101 alloy) and a liquid N_2 cold finger. Argon isotopic ratios (^{40}Ar-^{36}Ar) were measured with a Mass Analyzer Products 215 mass spectrometer with a Nier source and Balzers electron multiplier. Source and multiplier mass discrimination were determined after each step-heating run by measuring the $^{40}Ar/^{36}Ar$ ratio of 3×10^{-9} cm^3 (STP) of atmospheric argon. Extraction line blanks were measured every five steps. Typical line blanks measured during the runs were 2×10^{-16} mol for ^{40}Ar and 1×10^{-18} to 3×10^{-18} mol for ^{39}Ar, ^{38}Ar, ^{37}Ar, and ^{36}Ar. Total gas (integrated) ages incorporate all gas fractions released, and plateau ages were calculated as the inverse variance weighted mean of dates from steps in the plateau. Criteria used to define a plateau are that it include 50% or more of the total ^{39}Ar released in three or more consecutive steps and that the ages of all steps overlap at 2σ. Replicates of each sample were run to evaluate reproducibility and grain to grain variability between analyses.

Sample Description

Universal transverse mercator (UTM) coordinates of samples analyzed are listed in Table 1. Compositions of minerals analyzed for $^{40}Ar/^{39}Ar$ dates are reported in Tables 2 and 3. Hornblende was extracted from amphibolites composed of hornblende, plagioclase, quartz, ±biotite, and accessory minerals. Amphiboles had no observable retrograde alteration in backscattered electron images and are classified as hornblendes according to the classification scheme of *Leake* [1978] (ferroan-pargasitic-, ferro-tschermakitic-, tschermakitic-, and magnesio-hornblendes, specifically) with $Mg/(Mg+Fe^{2+})$ from 0.41 to 0.52. Maximum grain sizes (prism width) observed in thin section were 150 to 250 μm. The size fraction of separates obtained was 180 to 300 μm. Phlogopite grains were hand picked from crushed coarse-grained calcitic marbles. Phlogopites have only 1-4% annite but contain 22-51% F/[F+OH]. Euhedral, unbroken grains selected for analysis ranged from 650 to 1000 μm in diameter (plate breadth). Biotite sample RVL20B was obtained from an amphibolite. Biotite from a 200 μm size fraction has 55% annite. Slight chlorite alteration of some grains was observed in thin section, which were avoided during sample selection. Biotite-muscovite-quartz-plagioclase-sillimanite schist (sample LVT130A) and pegmatite mylonite (sample SRD104) were processed for muscovite separates that were 1000 to 1300 μm in diameter. Muscovites contain 6.1 and 6.3 Si^{iv} per formula unit and Na/(Na+K) of 0.05 and 0.13.

Table 1. Universal Transverse Mercator Grid Coordinates of Samples (Grid Zone 18T) and Summary of Sample Descriptions and Ages

Sample	Northing	Easting	Rock Type	Mineral	Domain	t_p, Ma	t_t, Ma	T_c, °C
RVL118A	4971225	372600	amphibolite	hornblende	SL	1011±2	1009±2	480
RVL20A	4973050	367025	amphibolite	hornblende	SL	1205±2	1212±2	
CDN58	4968970	356050	amphibolite	hornblende	M	947±1	952±2	490
JOL164	5003920	370350	amphibolite	hornblende	M	940±2	944±2	475
MTG72	4957060	355300	amphibolite	hornblende	M	952±1	966±2	485
DHL251	4983180	381360	marble	phlogopite	M	983±1	983±2	410
MTG175	4952250	356290	marble	phlogopite	SL	1014±1	1023±2	410
RVL20B	4973050	367025	amphibolite	biotite	SL	1034±2	1029±2	270
BTN195	5026550	376720	marble	phlogopite	M	907±1	905±2	395
ARN191	5032900	384850	marble	phlogopite	M	912±2	910±2	380
ARN199	5032900	384870	marble	phlogopite	SZ	927±1	924±1	400
LVT130A	4990750	361920	schist	muscovite	M	893±1	893±1	320
SRD104	4978060	367720	pegmatite	muscovite	SZ	889±1	890±1	330
RVL118B*	4971225	372600	amphibolite	biotite	SL	986±1	969±1	295
LVT130B*	4990750	361920	schist	biotite	M	901±1	901±1	340

M is Mazinaw domain; SL is Sharbot Lake domain; SZ is shear zone; t_p is plateau age; t_t is total gas (integrated) age, errors are 1σ, closure temperatures are the mean value calculated using grain sizes of samples, cooling rates for the Grenville Province, and experimental data from literature (see text for references).

*Data taken from *Busch et al.*[1995].

Table 2. Hornblende Compositions Determined by Electron Microprobe Analysis

Wt% oxide	RVL118A	RVL20A	CDN58	JOL164	MTG72
SiO_2	41.35	46.10	41.78	44.93	42.66
Al_2O_3	13.96	8.52	12.95	10.59	10.58
TiO_2	0.58	1.30	0.85	0.78	1.13
Fe_2O_3	6.73	4.57	3.52	4.16	5.81
FeO	14.04	14.69	16.98	14.98	14.38
MnO	0.34	0.39	0.28	0.19	0.24
MgO	7.02	9.30	6.77	9.03	8.51
Cr_2O_3	0.01	0.01	0.06	0.01	0.00
CaO	10.99	11.28	11.58	11.87	11.31
Na_2O	1.64	1.12	1.32	1.12	1.74
K_2O	0.77	0.47	1.14	0.26	0.58
F	0.24	0.08	0.03	0.10	0.06
Cl	0.48	0.05	0.02	0.00	0.17
H_2O^*	1.98	2.22	2.22	2.23	2.17
$O=F^*$	-0.10	-0.03	-0.01	-0.04	-0.02
$O=Cl^*$	-0.11	-0.01	-0.01	0.00	-0.04
Total	99.91	100.06	99.48	100.19	99.28

*Determined from mineral formulae normalized to 13 small cations.

Closure Temperatures

To define cooling histories (temperature-time paths), the closure temperature of individual minerals must be known. Closure temperatures depend on mineral diffusion parameters such as activation energy, frequency factor, as well as grain (diffusion domain) size, and cooling rate [*Dodson*, 1973, 1979]. Varied field and laboratory based experimental results for activation energy and frequency factor have lead to a wide range of closure temperatures for hornblende and micas [*Giletti*, 1974; *Harrison and McDougall*, 1980; *Harrison*, 1981; *Harrison et al.*, 1985; *Hammerschmidt and Stöckhert*, 1987; *Snee et al.*, 1988; *Baldwin et al.*, 1990; *Hames and Bowring*, 1994].

To provide the most conservative estimate of closure temperatures for minerals of interest in this study experimental data were compiled and closure temperatures calculated using the formulation of *Dodson* [1973, 1979]. Mica grain morphological characteristics were used to select single, unbroken grains and plate diameters were measured. Due to difficulty in determining the degree of crushing of individual hornblende grains, grain size estimates from thin sections were used in calculating closure temperature. Because the grain size is not necessarily the diffusion domain size, the measured grain sizes are used as the maximum diffusion domain sizes and the minimum domain sizes are arbitrarily taken as half the measured grain sizes. Diffusion domain radii used for hornblendes are 40-125 μm, which encompasses the minimum

Table 3. Mica Compositions Determined by Electron Microprobe Analysis

Wt% oxide	DHL251 Phlogopite	MTG175 Phlogopite	RVL20B Biotite	BTN195 Phlogopite	ARN191 Phlogopite	ARN199 Phlogopite	LVT130A Muscovite	SRD104 Muscovite
SiO_2	40.11	40.63	35.41	41.34	42.60	42.43	44.47	45.37
TiO_2	0.23	0.82	1.92	0.49	0.69	0.65	0.41	0.66
Al_2O_3	13.17	14.11	16.15	12.81	11.58	11.96	34.00	30.78
Cr_2O_3	0.02	0.07	0.10	0.02	0.01	0.00	0.07	0.01
FeO	0.58	0.59	20.87	0.88	1.04	2.05	2.71	4.62
MnO	0.00	0.00	0.20	0.06	0.03	0.00	0.00	0.03
MgO	27.59	27.41	9.75	27.05	27.45	26.91	0.78	1.17
BaO	0.63	0.00	0.31	0.58	1.32	0.00	0.18	0.13
CaO	0.01	0.09	0.01	0.08	0.01	0.02	0.02	0.00
Na_2O	0.67	0.22	0.06	0.74	0.42	0.35	0.95	0.32
K_2O	9.66	10.33	9.20	9.07	8.99	9.68	9.64	10.73
F	4.34	1.98	0.28	4.39	4.18	3.45	0.07	0.16
Cl	0.00	0.25	0.00	0.00	0.04	0.02	0.00	0.00
H_2O^*	2.12	3.25	3.78	2.12	2.23	2.59	4.44	4.33
$O=F^*$	-1.83	-0.83	-0.12	-1.85	-1.76	-1.45	-0.03	-0.07
$O=Cl^*$	0.00	-0.06	0.00	0.00	-0.01	0.00	0.00	0.00
Total	97.30	98.86	97.92	97.79	98.82	98.65	97.71	98.25

*Determined from mineral formulae normalized on the basis of 24 (O+OH+F+Cl).

domain sizes inferred from experimental work [*Harrison and McDougall,* 1980; *Harrison*, 1981]. Mica diffusion domain radii are generally taken as the grain radii [*Giletti*, 1974; *Hames and Bowring*, 1994], although there is some evidence for an intrinsic diffusion radius of 150-200 μm for biotite [*Harrison et al.*, 1985]. Using diffusion domain radii of 50-100 μm, 250-650 μm, and 100-500 μm for biotite, muscovite, and phlogopite, respectively, encompasses the experimental constraints on diffusion domain sizes for micas. Previous studies have defined the cooling rate for the Metasedimentary Belt at 1°-5°C/m.y. [*Hanes et al.*, 1988; *Cosca et al.*, 1991]. Closure temperatures were calculated for each sample, the mean value is taken as the closure temperature, and the minimum and maximum values are used to bracket the errors. Closure temperatures may also depend on mineral composition, although there is currently no consensus on the influence of composition or quantitative means of correcting closure temperature for composition [*O'Nions et al.*, 1969; *Harrison et al.*, 1985; *Grove and Harrison,* 1993; *Cosca and O'Nions*, 1994]. The closure temperatures used lie in the ranges of 475°-490°C, 380°-410°C, 320°-330°C, and 270°-340°C for hornblende, phlogopite, muscovite, and biotite, respectively (Table 1).

The $^{40}Ar/^{39}Ar$ Results

Twenty-one samples were analyzed for $^{40}Ar/^{39}Ar$ age determinations. Each sample was run in duplicate to ensure reproducibility, and occasionally triplicate or quadruplicate analyses were run. Thirteen samples had reproducible spectra with similar total gas and plateau ages (Table 1 and Figure 2). Eight samples that are not presented here do not have spectral plateaus; they are not reproducible and have total gas ages 80 to 250 Ma older than other cooling ages in the region. Four of these samples, which were located in the shear zone and were extracted from mylonites, are interpreted to have incorporated excess argon during late deformation. The other four were phlogopite samples; one sample located in the northern Sharbot Lake domain near the village of Packenham recorded integrated ages from 1256 to 1306 Ma perhaps reflecting crystallization ages in the region [*Corfu and Easton*, 1994]. The ^{36}Ar content of these samples is too low to provide meaningful isochrons ($^{36}Ar/^{40}Ar$ versus $^{39}Ar/^{40}Ar$). Isotope correlation diagrams ($^{39}Ar/^{40}Ar$ versus $^{37}Ar/^{40}Ar$ and $^{38}Ar/^{40}Ar$) indicate that there is no systematic correlation between Ca or Cl content and age. The ages are interpreted in the context of regional metamorphism and generally yield cooling ages. Because the equation for closure temperature of *Dodson* [1973, 1979] was formulated using total gas (integrated) ages for undisturbed samples, integrated ages are taken as cooling ages whenever possible. For spectra that are irregular due to excess Ar in low temperature steps for example, plateau ages are taken as cooling ages.

Hornblende $^{40}Ar/^{39}Ar$ data from two samples taken from the Sharbot Lake domain are listed in Table 4 and the associated age spectra are shown in Figures 2a and 2b. Step-heating data commonly show a component of excess Ar for the first percent of gas released. Sample RVL118A has a spectrum with progressively older ages at higher temperature steps, indicative of Ar loss during slow cooling. Therefore the total gas age is used as the cooling age (Figure 2a). An extremely old age (1212 Ma total gas age) was obtained from sample RLV20A, which was separated from an epidote-amphibolite metavolcanic rock in the hanging wall adjacent to the shear zone (Figure 2b). The age spectrum is reproducible but does not yield a plateau age based on the established criteria because one step is 3 m.y. too young. However, the spectrum is relatively simple, and based on other geologic evidence this age is likely to be meaningful: the outcrop from which this sample was taken is adjacent to the 1210-1225 Ma Lavant gabbro complex and the peak metamorphic temperatures in the region are low (~500°C) [*Corfu and Easton*, 1994; *Busch et al.* 1995]. The preferred $^{40}Ar/^{39}Ar$ age (1205 Ma) is interpreted to reflect amphibole growth or cooling of the metavolcanic unit during or immediately after emplacement of the Lavant gabbro. Because rocks in the hanging wall adjacent to the shear zone have not experienced high-grade metamorphism, cooling ages in amphiboles cannot be obtained in this region.

Release spectra from three hornblende samples from the Mazinaw domain are shown in Figures 2c-2e. Sample CDN58 has a release spectrum indicative of excess Ar over the first 30% of ^{39}Ar release, which suggests that the integrated age obtained from this sample may be anomalously old (Figure 2c). Similarly, sample MTG72 has a saddle shaped spectrum from which the cooling age is inferred from the plateau age (Figure 2e). Plateau ages are used as cooling ages for samples CDN58, MTG72, and JOL164 due to the irregular age spectra of these samples (Figures 2c, 2d, and 2e). The Ca/K spectra sympathetically follow the age spectra for two of these samples (Figures 2d and 2e), which may reflect optically undetectable exsolution lamellae [*Harrison and Fitz Gerald*, 1986]. Given the low K concentrations and precision of the electron microprobe technique, electron microprobe Ca/K ratios of hornblendes are compatible with Ca/K ratios obtained from Ar isotopic ratios (Figures 2a-2e). The ages obtained are consistent with presently available hornblende data in the region [*Cosca et al.*, 1991, 1992]. The data indicate that the Mazinaw domain passed through the closure temperature for Ar in hornblende at 920-950 Ma. In contrast, the Sharbot Lake domain cooled through 480°C at 1007-1009 Ma (Figure 3).

A variety of micas were analyzed, and the $^{40}Ar/^{39}Ar$ data are listed in Table 5 with associated spectra in Figure 2. Most micas have plateau ages slightly younger or analytically indistinguishable from total gas ages. Therefore the total gas ages are used as cooling ages except for sample MTG175, which has a saddle-shaped spectrum, and the plateau age is taken as the cooling age (Figure 2g). The age obtained for sample MTG175 is older than a nearby hornblende cooling age, which makes this cooling age suspect (Figure 3). Phlogopites generally have uniform ages for the entire ^{39}Ar release. Sample ARN199 was extracted from mylonite in the shear zone and has an integrated age 14±3 Ma older than that of sample ARN191, which was extracted from the protolith marble in the same outcrop (Figures 2j and 2k). This difference may be a reflection of incorporation of excess Ar in the mylonitic sample but is not reflected in the spectrum. The Mazinaw domain passed through the Ar closure temperature for phlogopite at 905-924 Ma, while the Sharbot Lake domain passed through 410°C by 983 Ma (Figure 3).

Analyses of two muscovite samples indicate that the Mazinaw domain reached 320-330°C at 890-893 Ma (Figure 2l

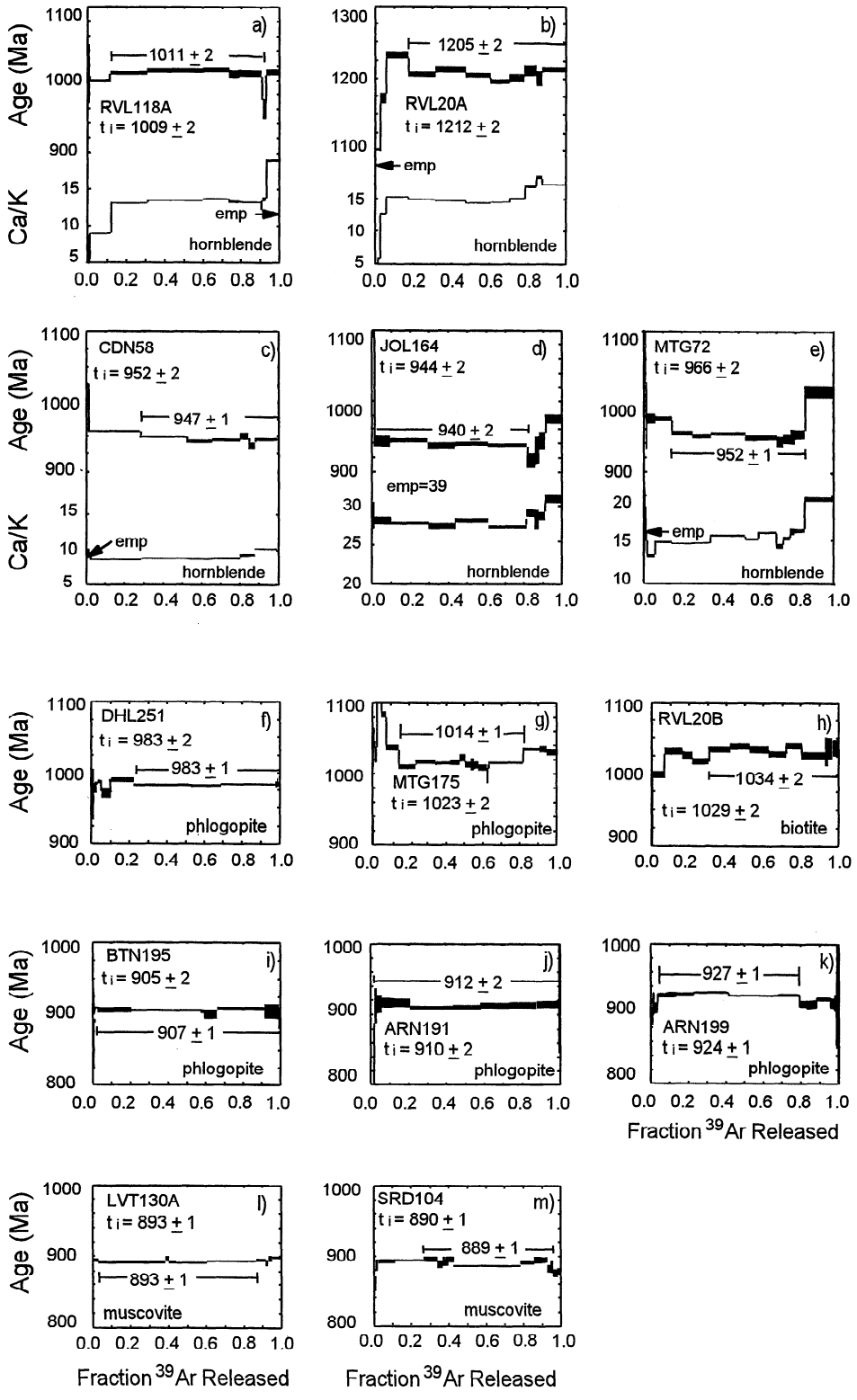

Figure 2. Argon release spectra for hornblende, phlogopite, biotite, and muscovite constructed using data in Tables 4 and 5. Spectra in Figures 2a, 2b, and 2f-2h are from samples in the Sharbot Lake domain. Width of steps and reported errors are $\pm 1\sigma$. Symbol t_i refers to total gas (integrated) age. Abbreviation emp refers to Ca/K ratios determined by electron microprobe analyses (hornblende mineral formulae normalized to 13 small cations).

Table 4. Argon Isotope Data Obtained During Hornblende Step Heating Runs

Power mW	^{39}Ar Fraction	$^{39}Ar_K$ Moles	$^{40}Ar/^{39}Ar$	$^{38}Ar/^{39}Ar$	$^{37}Ar/^{39}Ar$	$^{36}Ar/^{39}Ar$	$^{40}Ar^*/^{39}Ar_K$	Ca/K	% ^{40}Ar Atmos.	Age, Ma	error 1σ, Ma
					RVL118A Hornblende (200 μm)						
100	0.003	1.412E-14	156.2	1.647	5.27	0.214	92.9	9.7	40.4	882	85
240	0.012	6.322E-14	129.7	0.731	2.81	0.057	112.9	5.2	12.9	1026	23
360	0.121	6.105E-13	110.3	2.539	4.88	0.005	108.9	9.0	1.2	998	2
420	0.312	1.580E-12	111.2	3.392	7.18	0.002	110.5	13.2	0.5	1010	2
440	0.602	3.051E-12	111.6	3.663	7.39	0.002	111.0	13.6	0.4	1013	3
460	0.738	3.738E-12	111.7	3.612	7.51	0.002	111.2	13.8	0.4	1014	4
480	0.794	4.021E-12	111.9	3.697	7.30	0.005	110.4	13.4	1.3	1009	5
520	0.908	4.598E-12	111.4	3.551	7.25	0.003	110.5	13.3	0.8	1009	4
560	0.917	4.646E-12	113.3	2.959	7.03	0.019	107.6	12.9	5.0	989	16
680	0.935	4.734E-12	108.8	3.030	7.49	0.019	103.3	13.8	5.0	958	12
2000	1.000	5.065E-12	112.1	3.293	10.39	0.005	110.7	19.1	1.2	1011	4
					RVL20A Hornblende (200 μm)						
80	0.002	7.082E-15	1509.0	6.466	3.61	3.098	593.6	6.6	60.7	2739	138
160	0.005	1.826E-14	419.8	2.553	1.89	0.593	244.5	3.5	41.8	1630	76
280	0.008	3.266E-14	307.9	1.299	1.93	0.372	198.1	3.5	35.7	1414	55
400	0.016	6.412E-14	192.4	0.731	1.92	0.211	130.1	3.5	32.4	1041	25
480	0.027	1.070E-13	148.9	0.681	3.11	0.051	133.8	5.7	10.2	1063	28
560	0.058	2.324E-13	156.7	1.089	6.90	0.015	152.3	12.7	2.8	1172	7
680	0.176	7.011E-13	164.8	1.152	8.30	0.006	163.1	15.2	1.0	1232	5
760	0.317	1.267E-12	159.6	1.080	8.11	0.004	158.4	14.9	0.7	1206	3
840	0.477	1.903E-12	161.2	1.102	7.99	0.005	159.7	14.7	0.9	1213	4
920	0.607	2.424E-12	159.6	1.044	7.81	0.004	158.2	14.3	0.8	1205	3
1000	0.705	2.815E-12	158.2	1.039	7.87	0.005	156.6	14.4	1.0	1196	3
1100	0.784	3.132E-12	158.9	1.078	8.22	0.005	157.5	15.1	0.9	1200	5
1240	0.846	3.378E-12	160.9	1.155	9.24	0.005	159.5	17.0	0.9	1211	8
1400	0.876	3.498E-12	159.1	1.148	9.99	0.006	157.3	18.3	1.1	1200	11
3000	1.000	3.993E-12	161.1	1.145	9.39	0.005	159.7	17.2	0.8	1213	4
					CDN58 Hornblende (250 μm)						
200	0.003	3.837E-14	370.6	1.152	9.11	0.807	132.1	16.7	64.3	1168	38
400	0.017	2.537E-13	133.5	0.243	5.50	0.071	112.6	10.1	15.6	1036	7
520	0.285	4.359E-12	102.1	0.143	4.85	0.002	101.6	8.9	0.5	958	1
560	0.525	8.047E-12	100.7	0.143	4.93	0.001	100.5	9.1	0.2	949	1
600	0.662	1.014E-11	100.3	0.141	4.91	0.002	99.7	9.0	0.5	944	2
680	0.806	1.234E-11	100.4	0.140	4.96	0.001	100.0	9.1	0.4	946	2
760	0.849	1.300E-11	101.4	0.146	5.16	0.002	100.7	9.5	0.6	951	5
900	0.883	1.352E-11	99.3	0.149	5.20	0.001	98.9	9.5	0.3	938	5
3000	1.000	1.531E-11	100.6	0.149	5.67	0.002	100.1	10.4	0.4	947	2
					JOL164 Hornblende (170 μm)						
80	0.002	6.410E-15	247.5	0.901	29.65	0.345	145.5	54.4	41.1	1294	146
160	0.012	4.011E-14	136.4	0.210	15.81	0.057	119.5	29.0	12.3	1121	32
200	0.099	3.246E-13	96.5	0.043	15.39	0.004	95.1	28.2	1.3	942	8
240	0.296	9.728E-13	95.5	0.047	15.22	0.001	95.3	27.9	0.2	944	3
260	0.438	1.443E-12	95.4	0.046	15.02	0.003	94.4	27.6	1.0	936	5
300	0.615	2.022E-12	95.4	0.045	15.47	0.002	94.7	28.4	0.7	939	3
360	0.817	2.687E-12	95.0	0.044	14.94	0.002	94.4	27.4	0.6	937	3
420	0.860	2.831E-12	93.4	0.058	16.04	0.006	91.8	29.4	1.7	916	10
500	0.881	2.899E-12	95.3	0.057	15.53	0.006	93.6	28.5	1.7	931	19
600	0.914	3.006E-12	95.7	0.043	15.80	0.001	95.3	29.0	0.4	943	13
2000	1.000	3.290E-12	100.6	0.047	17.12	0.004	99.4	31.4	1.1	975	7

Table 4. (continued)

Power mW	^{39}Ar Fraction	$^{39}Ar_K$ Moles	$^{40}Ar/^{39}Ar$	$^{38}Ar/^{39}Ar$	$^{37}Ar/^{39}Ar$	$^{36}Ar/^{39}Ar$	$^{40}Ar^*/^{39}Ar_K$	Ca/K	% ^{40}Ar Atmos.	Age, Ma	error 1σ, Ma
					MTG72 Hornblende (230 μm)						
100	0.004	2.469E-14	209.2	1.312	6.55	0.223	143.3	11.9	31.5	1231	50
200	0.011	6.953E-14	192.3	1.132	9.67	0.257	116.5	17.8	39.4	1056	29
300	0.019	1.226E-13	138.6	1.156	7.78	0.124	101.9	14.3	26.5	953	22
400	0.060	3.767E-13	113.9	1.541	6.87	0.030	105.1	12.7	7.7	976	8
450	0.148	9.359E-13	107.1	1.813	7.54	0.007	105.1	13.8	1.8	976	3
480	0.258	1.633E-12	103.6	1.797	7.47	0.005	102.2	13.8	1.4	955	3
520	0.355	2.245E-12	102.8	1.761	7.50	0.004	101.6	14.3	1.2	951	3
560	0.537	3.397E-12	102.8	1.798	7.85	0.002	102.1	14.3	0.7	954	3
580	0.606	3.834E-12	102.8	1.775	7.68	0.005	101.3	14.1	1.4	949	4
620	0.703	4.447E-12	102.6	1.782	7.98	0.004	101.3	14.7	1.2	949	3
660	0.738	4.668E-12	101.5	1.793	7.35	0.004	100.4	13.6	1.1	942	7
720	0.776	4.907E-12	102.0	1.713	7.73	0.003	101.1	14.1	0.9	947	7
800	0.796	5.031E-12	102.5	1.802	8.04	0.003	101.5	14.7	1.0	950	11
960	0.850	5.372E-12	102.8	1.809	8.09	0.003	101.9	14.9	0.9	953	6
2000	1.000	6.322E-12	111.8	1.828	9.63	0.004	110.5	17.6	1.2	1015	8

Columns are, from left to right, laser power (beam diameter 1.5 mm); cumulative fraction ^{39}Ar released; moles of K-derived ^{39}Ar in step; isotopic ratios corrected for blank, mass discrimination, Ca-, K-, and Cl-derived Ar isotopic interference, decay of ^{37}Ar, and ^{36}Ar from decay of ^{36}Cl; ratio of radiogenic ^{40}Ar to K-derived ^{39}Ar; weight ratio calculated using Ca/K = 1.835 X ($^{37}Ar_{Ca}/^{39}Ar_K$); % ^{40}Ar atmospheric of total ^{40}Ar in fraction; apparent ages calculated using decay constants recommended by *Steiger and Jäger* [1977]; error includes uncertainties in J, mass discrimination, blank, and isotopic measurements. Reported errors are 1σ. Grain sizes are the maximum size observed in thin section. For RVL118A $J = 0.00678333 \pm 0.00001291$, total gas age is 1009 ± 2 Ma, plateau age (420-560) is 1011 ± 2 Ma (mswd = 0.8). For RVL20A $J = 0.00600314 \pm 0.00001205$, total gas age is 1212 ± 2 Ma, preferred age (760-3000) is 1205 ± 2 Ma (mswd = 2.7). For CDN58 $J = 0.00689001 \pm 0.00001731$, total gas age is 952 ± 2 Ma, plateau age (560-3000) is 947 ± 2 Ma (mswd = 2.7). For JOL164 $J = 0.00720491 \pm 0.00000892$, total gas age is 944 ± 2 Ma, plateau age (200-360) is 940 ± 2 Ma (mswd = 1.1). For MTG72 $J = 0.00682940 \pm 0.00001438$, total gas age is 966 ± 2 Ma, plateau age (480-960) is 952 ± 1 Ma (mswd = 0.7).

and 2m). These ages are 10 m.y. younger than the biotite datum in the Mazinaw domain [*Busch and van der Pluijm,* 1995], reflecting the overlapping closure temperatures for muscovite and biotite. One biotite sample was analyzed in the Sharbot Lake domain (Figure 2h). Argon loss is indicated by the first 7% of gas release. The age spectrum is slightly irregular; however, a plateau is present over 70% of the release spectrum and the total gas age and plateau age overlap at 2σ. This age indicates that the western portion of the Sharbot Lake domain passed through 310°C at 1029 Ma, in sharp contrast to the older amphibole growth age in this sample (RLV20A) and younger biotite and hornblende cooling ages farther to the east (Figure 3).

Discussion

Cooling Histories

The cooling histories of the Mazinaw and Sharbot Lake domains may be calculated by combining closure temperatures and cooling ages. Cooling curves for each domain are constructed by plotting the Ar closure temperature versus cooling age (Figure 4). The age and temperature of metamorphism are used as the starting point for the temperature-time (T-t) curves and the crosscutting dikes of the Grenville dike swarm (590 Ma) [*Kamo et al.,* 1995], and the Paleozoic unconformity constrain the end points of the cooling curves. All available data for the two domains are incorporated in the temperature-time paths (Figure 4).

The last metamorphism in the Mazinaw domain has been dated at 1012-1052 Ma using U/Pb data from zircon and sphene [*Mezger et al.*, 1991; *Corfu and Easton,* 1995]. Metamorphic temperatures of the Mazinaw domain are 550°-650°C [*Hutcheon and Moore*, 1973; *Sethuraman and Moore*, 1973; Carmichael et al., 1978; *Cureton*, 1994; *Busch et al.*, 1995]. The Mazinaw domain experienced a period of slow cooling (2°C/m.y.) following metamorphism. Cooling rates increase to 4°-5°C/m.y. during the period from 950 to 890 Ma. The cooling history is constrained at the end of cooling by the presence of shallow level 590 Ma dikes and Cambrian to Ordovician sedimentary rocks that unconformably overlie Proterozoic metamorphic rocks in the area [*Kamo et al.*, 1995]. Thus the Proterozoic metamorphic rocks were at or near the earth's surface by 590 Ma. It is likely that the cooling rate from 890 Ma to 590 Ma was not constant but gradually decreased from 5°C/m.y. to <1°C/m.y. over this interval. Therefore cooling curves are constructed to reflect smoothly decreasing cooling rates for this time period (Figure 4).

The age of metamorphism in the Sharbot Lake domain is constrained by sphene and zircon U/Pb dates of ~1160 Ma and sphene and zircon dates in the range of 1210-1240 Ma, which suggest that the Sharbot Lake domain has not experienced the late (1012- 1052 Ma) metamorphism [*Mezger et al.*, 1991;

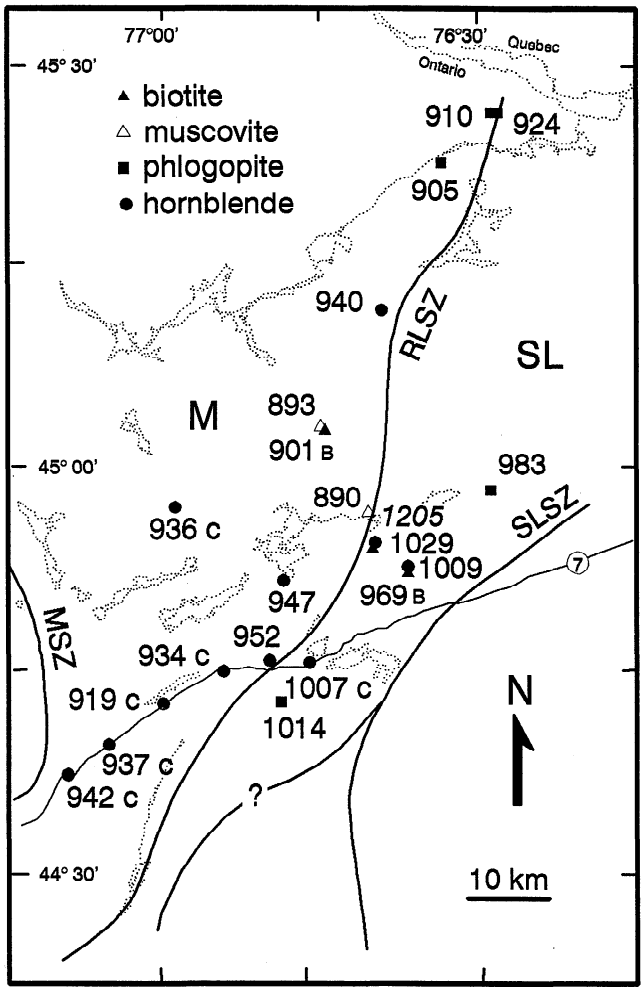

Figure 3. Map showing locations of $^{40}Ar/^{39}Ar$ ages in the region. Ages denoted with C and B are from *Cosca et al.* [1991, 1992] and *Busch and van der Pluijm* [1995], respectively. Major lakes and rivers (dotted lines) and Ontario highway 7 are shown for reference. The italicized date is a growth age. Shear zone abbreviations are given in Figure 1.

Corfu et al., 1995]. The amphibole growth age (sample RVL20A) that records the emplacement of the Lavant gabbro further demonstrates the lack of metamorphism (or shallow structural levels) in the hanging wall adjacent to the RLSZ since circa 1205 Ma. Peak metamorphic temperatures in the Sharbot Lake domain vary from 500°C to 750°C from west to east [*Busch et al.*, 1995]. Thus the starting point for cooling curves in the Sharbot Lake domain varies depending on the location within the domain (Figure 4). Metamorphism was followed by a period of slow cooling (~2°C/m.y.) until ~1010 Ma. Hornblende and biotite cooling ages from sample RVL118 yield a cooling rate of 5°C/m.y. from 969 to 1009 Ma for the central Sharbot Lake domain using closure temperatures of 295°C and 480°C calculated for these samples. Samples RVL20A-B, MTG175, and DHL251 do not lie along the cooling curve derived from samples RVL118A-B, suggesting that the cooling history varied across the Sharbot Lake domain. The western Sharbot Lake domain was already well below the closure temperature for biotite when the central portion of the domain was undergoing rapid cooling from 500°C to 300°C. Subsequently, the cooling rate decreased to <1°C/m.y as the rocks reached the surface (Figure 4).

Unroofing History

A cooling age (t_c) can be used to calculate the depth of the rock at time t_c by dividing the closure temperature by an assumed geothermal gradient. A model geothermal gradient of 25°C/km is used as a reference gradient; because the relative unroofing across the region is of interest, the absolute magnitude of the gradient chosen is not critical. The depths of rocks with different cooling ages can be computed at a reference time by extrapolating temperature through time along a cooling curve. The cooling curves used to extrapolate depth through time are shown as dashed lines on the T-t plot (Figure 4). The unroofing history is defined by calculating the depths of rocks in the area at different times. The underlying assumptions are that the isotherms remained essentially horizontal and the geothermal gradient is uniform and linear throughout the area.

In the Mazinaw domain, hornblende cooling ages are used to compute the depths of rocks at 950 Ma. Because hornblende cooling ages are near 950 Ma, extrapolations of depths are not great and thus errors in cooling rate have only a minor effect on depth. For example, a 2°C/m.y. error in cooling rate extrapolated 30 m.y. translates to an error of 2.4 km depth using a geothermal gradient of 25°C/km. The differences in hornblende cooling ages within the Mazinaw domain lead to a range of calculated depths (Figure 5) that do not correlate spatially to geologic structures, suggesting that the differences may be due to inherent differences between samples (i.e., late deformation, alteration, or mineral chemistry). For comparison, the depths of these samples at 1000 Ma are determined by extrapolation of hornblende data using a cooling rate of 2°C/m.y. (Figure 5). The data on metamorphic pressures indicate that depths of metamorphism were 20-25 km over most of the domain [*Busch et al.*, 1995], which is generally consistent with this extrapolation. The 900 Ma depths (~14 km) are determined by cooling dates from micas.

East of the RLSZ, the unroofing history is drastically different. Hornblende and mica cooling ages are used to determine depths at 1000 Ma. Mica cooling ages provide data for the 950 Ma depths. These depth calculations indicate a difference in unroofing history across the Sharbot Lake domain. One biotite sample near the RLSZ (RVL20B) indicates shallow depths (<12 km) for the hanging wall adjacent to the RLSZ since 1029 Ma. This inference is corroborated by the amphibole growth age from this sample (RVL20A), which suggests that this portion of the domain has been at shallow (cooler) structural levels since 1205 Ma. Sample DHL251 is the easternmost sample analyzed, and it lies along a cooling curve that corresponds to the greatest depths in the Sharbot Lake domain. There are no data to construct depths in the Sharbot Lake domain at 900 Ma. The lack of cooling dates from samples with a lower closure temperature precludes the interpretation of convergence of the cooling curves in the Sharbot Lake domain. However, the different depths must have been accommodated by differential unroofing by 590 Ma.

Table 5. Argon Isotope Data Obtained During Mica Stcp Heating Runs

Power mW	^{39}Ar fraction	$^{39}Ar_K$ Moles	$^{40}Ar/^{39}Ar$	$^{38}Ar/^{39}Ar$	$^{37}Ar/^{39}Ar$	$^{36}Ar/^{39}Ar$	$^{40}Ar^*/^{39}Ar_K$	% ^{40}Ar Atmos.	Age, Ma	error 1σ, Ma
				DHL251 Phlogopite (1000 μm)						
360	<0.001	1.861E-14	43.0	0.031	-0.93	0.075	20.8	51.5	243	212
480	<0.001	2.900E-14	82.4	-0.013	1.32	0.089	56.1	31.8	592	212
660	<0.001	6.527E-14	109.6	0.024	0.44	0.029	101.0	7.8	957	48
800	0.001	1.123E-13	111.4	-0.008	-0.43	0.027	103.5	7.1	975	41
900	0.001	1.905E-13	105.7	0.016	0.13	-0.004	107.0	-1.2	1000	18
980	0.001	2.093E-13	156.4	0.047	-1.57	0.162	108.5	30.6	1011	74
1120	0.002	3.173E-13	101.4	0.021	0.10	0.004	100.1	1.2	950	16
1200	0.002	4.038E-13	105.0	0.029	0.09	0.013	101.1	3.7	957	20
1320	0.004	7.150E-13	102.8	0.022	0.02	0.003	102.0	0.8	964	7
1400	0.007	1.150E-12	102.6	0.018	0.00	0.003	101.8	0.7	963	5
1500	0.008	1.368E-12	103.5	0.018	-0.11	0.006	101.6	1.8	961	6
1680	0.016	2.707E-12	104.3	0.019	0.00	0.001	103.9	0.4	978	2
1750	0.038	6.306E-12	105.1	0.018	0.00	0.001	104.9	0.1	985	2
1760	0.050	8.350E-12	105.4	0.017	0.00	0.000	105.3	0.0	988	2
1761	0.060	9.995E-12	105.6	0.017	0.00	0.000	105.5	0.1	989	1
1762	0.109	1.811E-11	103.2	0.017	-0.00	0.000	103.1	0.1	972	7
1763	0.230	3.804E-11	105.7	0.017	0.00	0.000	105.6	0.0	990	3
1764	0.533	8.831E-11	104.5	0.015	0.00	0.000	104.5	0.0	982	2
1765	0.695	1.151E-10	104.6	0.015	0.00	0.000	104.5	0.01	982	2
1766	0.984	1.630E-10	104.8	0.015	0.00	0.000	104.8	0.1	984	1
1767	0.990	1.641E-10	105.1	0.017	-0.02	0.001	104.8	0.32	984	4
1900	0.992	1.644E-10	105.9	0.022	-0.06	0.003	105.1	0.7	986	6
4000	1.000	1.657E-10	105.0	0.015	-0.02	0.001	104.8	0.2	984	3
				MTG175 Phlogopite (1000 μm)						
160	0.001	2.000E-14	85.5	0.028	0.13	0.049	70.9	17.1	746	131
240	0.003	6.214E-14	105.5	0.064	0.10	0.022	99.0	6.2	973	36
320	0.013	2.403E-13	111.0	0.052	0.01	0.003	110.1	0.8	1055	10
400	0.025	4.579E-13	108.8	0.050	-0.01	0.009	106.1	2.4	1026	10
480	0.049	8.907E-13	123.4	0.056	-0.00	0.006	121.5	1.6	1136	7
520	0.076	1.365E-12	115.4	0.054	0.00	0.004	114.1	1.1	1084	5
560	0.144	2.598E-12	108.4	0.055	-0.00	0.003	107.5	0.8	1036	4
570	0.236	4.264E-12	104.8	0.056	0.00	0.003	103.9	0.9	1010	3
571	0.345	6.220E-12	105.5	0.056	-0.00	0.002	104.8	0.6	1017	3
572	0.426	7.695E-12	105.5	0.058	-0.00	0.003	104.7	0.8	1015	2
573	0.473	8.532E-12	105.6	0.055	0.00	0.003	104.7	0.9	1015	4
574	0.507	9.140E-12	106.2	0.060	-0.00	0.002	105.6	0.5	1023	5
575	0.538	9.711E-12	105.0	0.055	0.00	0.002	104.3	0.7	1013	4
580	0.554	9.993E-12	105.4	0.057	-0.02	0.003	104.4	1.0	1014	8
590	0.578	1.043E-11	105.4	0.060	0.01	0.004	104.2	1.1	1012	5
600	0.623	1.124E-11	104.8	0.057	0.00	0.004	103.8	1.0	1009	5
610	0.632	1.141E-11	104.6	0.055	-0.01	0.008	102.2	2.3	997	11
630	0.821	1.482E-11	105.1	0.054	0.00	0.002	104.7	0.4	1015	2
880	0.909	1.640E-11	107.9	0.057	-0.00	0.002	107.3	0.6	1035	2
1000	0.948	1.711E-11	108.6	0.054	0.00	0.005	107.2	1.3	1034	4
1200	1.000	1.804E-11	107.6	0.051	0.00	0.003	106.6	0.8	1030	4

Table 5. (continued)

Power mW	^{39}Ar fraction	$^{39}Ar_K$ Moles	$^{40}Ar/^{39}Ar$	$^{38}Ar/^{39}Ar$	$^{37}Ar/^{39}Ar$	$^{36}Ar/^{39}Ar$	$^{40}Ar^*/^{39}Ar_K$	% ^{40}Ar Atmos.	Age, Ma	error 1σ, Ma
				RVL20B Biotite (200 μm)						
80	0.002	9.930E-15	55.0	0.159	1.56	-0.021	61.3	-11.4	633	121
200	0.070	3.491E-13	109.3	0.134	0.18	0.005	108.0	1.2	999	5
240	0.169	8.419E-13	113.3	0.130	-0.07	0.002	112.7	0.5	1033	4
280	0.218	1.091E-12	113.1	0.132	0.11	0.004	111.9	0.9	1027	5
360	0.306	1.527E-12	111.2	0.140	0.04	0.002	110.7	0.4	1019	4
440	0.421	2.104E-12	113.6	0.145	0.03	0.002	113.0	0.5	1034	4
520	0.528	2.637E-12	113.9	0.151	0.00	0.001	113.7	0.1	1039	4
600	0.629	3.143E-12	113.1	0.143	0.06	0.000	113.0	0.0	1035	4
680	0.720	3.596E-12	112.3	0.139	0.02	0.001	112.2	0.1	1029	4
760	0.807	4.032E-12	113.9	0.142	0.18	0.000	113.8	0.1	1040	4
840	0.933	4.661E-12	112.4	0.139	-0.00	0.002	111.9	0.4	1027	5
920	0.950	4.745E-12	110.9	0.140	-0.23	-0.006	112.7	-1.6	1032	20
1200	0.971	4.852E-12	112.3	0.135	-0.25	-0.003	113.2	-0.8	1036	15
2000	1.000	4.995E-12	114.1	0.146	-0.35	0.002	113.4	0.6	1037	12
				BTN195 Phlogopite (650 μm)						
400	<0.001	4.410E-14	71.4	0.412	23.11	0.145	28.4	60.1	316	42
500	<0.001	8.219E-14	109.0	0.266	76.13	0.063	90.5	16.9	858	35
600	0.001	1.312E-13	109.7	0.074	52.20	0.037	98.7	9.9	919	31
700	0.002	2.609E-13	102.7	0.020	7.47	0.012	99.1	3.5	922	12
800	0.005	8.170E-13	98.8	0.015	0.00	0.004	97.5	1.2	911	4
980	0.007	1.184E-12	97.6	0.013	-0.05	0.006	95.7	1.9	897	8
1000	0.011	1.882E-12	97.3	0.013	-0.04	0.001	96.8	0.4	906	4
1200	0.033	5.429E-12	97.5	0.013	0.00	0.001	97.3	0.2	909	1
1280	0.209	3.468E-11	96.9	0.009	0.00	0.000	96.9	0.1	906	4
1281	0.578	9.576E-11	96.8	0.009	0.00	0.000	96.8	0.1	905	1
1282	0.596	9.868E-11	97.0	0.010	0.01	0.002	96.6	0.4	904	3
1320	0.666	1.102E-10	96.2	0.009	0.00	0.000	96.1	0.1	900	6
1321	0.919	1.522E-10	97.2	0.010	0.003	0.000	97.1	0.0	908	2
1322	0.996	1.650E-10	96.8	0.012	0.00	0.000	96.7	0.1	904	10
1323	0.997	1.651E-10	93.3	0.017	-0.33	-0.007	95.3	-2.1	894	14
2000	1.000	1.656E-10	96.8	0.009	-0.07	-0.000	96.9	-0.1	906	5
				ARN191 Phlogopite (400 μm)						
160	0.020	9.365E-14	92.5	1.149	0.10	0.064	73.7	20.3	774	19
200	0.034	1.559E-13	93.7	0.016	0.00	0.010	90.7	3.2	913	25
280	0.064	2.943E-13	91.6	0.007	0.01	0.002	90.9	0.7	915	13
360	0.120	5.522E-13	92.3	0.008	0.00	0.004	91.1	1.2	916	7
440	0.216	9.907E-13	91.3	0.006	0.00	0.001	91.1	0.2	917	6
480	0.442	2.032E-12	91.0	0.005	0.00	0.003	90.2	0.8	910	3
481	0.588	2.700E-12	91.2	0.003	0.00	0.003	90.3	0.9	910	4
560	0.744	3.415E-12	91.4	0.005	0.00	0.003	90.6	0.8	913	4
580	0.880	4.042E-12	91.2	0.008	0.00	0.002	90.7	0.5	913	5
600	0.995	4.571E-12	91.3	0.008	0.00	0.002	90.9	0.5	915	5
620	1.000	4.592E-12	85.7	0.022	-0.03	-0.028	94.0	-9.6	939	92

Table 5. (continued)

Power mW	^{39}Ar fraction	$^{39}Ar_K$ Moles	$^{40}Ar/^{39}Ar$	$^{38}Ar/^{39}Ar$	$^{37}Ar/^{39}Ar$	$^{36}Ar/^{39}Ar$	$^{40}Ar^*/^{39}Ar_K$	% ^{40}Ar Atmos.	Age, Ma	error 1σ, Ma
				ARN199 Phlogopite (700 μm)						
80	0.001	1.228E-14	43.2	0.124	5.63	-0.031	52.2	-20.9	578	230
160	0.002	3.643E-14	106.4	0.067	0.74	0.049	91.9	13.7	919	58
240	0.012	1.999E-13	98.9	0.030	0.03	0.034	88.9	10.1	896	12
240	0.019	3.212E-13	96.1	0.010	0.00	0.016	91.3	5.0	914	16
280	0.038	6.325E-13	92.4	0.010	0.00	0.007	90.4	2.1	908	7
320	0.086	1.421E-12	93.7	0.010	0.00	0.003	92.8	1.0	926	3
340	0.139	2.284E-12	94.1	0.009	0.01	0.004	93.0	1.2	927	3
360	0.231	3.812E-12	93.5	0.008	0.00	0.002	92.9	0.6	927	2
370	0.415	6.845E-12	93.7	0.008	0.00	0.001	93.4	0.4	930	1
371	0.682	1.123E-11	93.0	0.009	0.00	0.001	92.7	0.3	926	1
372	0.794	1.308E-11	93.5	0.009	0.00	0.002	92.9	0.7	927	1
373	0.833	1.372E-11	92.2	0.007	-0.01	0.003	91.3	1.1	914	4
380	0.859	1.415E-11	92.7	0.012	-0.01	0.005	91.1	1.7	913	5
390	0.884	1.457E-11	91.9	0.007	-0.01	0.002	91.2	0.8	914	5
420	0.961	1.583E-11	92.5	0.009	0.02	0.001	92.2	0.3	921	2
430	0.980	1.615E-11	92.4	0.007	0.01	0.003	91.4	1.1	915	7
460	0.992	1.635E-11	92.3	0.007	0.35	0.003	91.4	1.0	915	11
500	0.995	1.639E-11	92.6	0.014	0.58	0.013	88.8	4.1	895	33
501	0.996	1.642E-11	91.9	-0.020	0.98	-0.009	94.5	-2.9	939	70
560	0.998	1.645E-11	93.4	-0.011	3.65	0.013	89.5	4.2	900	48
720	0.999	1.647E-11	98.6	-0.034	0.29	0.035	88.3	10.5	891	93
2000	1.000	1.648E-11	89.5	0.007	7.90	0.020	83.7	6.5	854	104
				LVT130A Muscovite (1000 μm)						
60	<0.001	7.314E-15	101.3	0.202	5.69	0.317	7.7	92.3	99	349
100	<0.001	1.131E-14	159.6	0.253	9.13	0.485	16.2	89.8	200	469
140	0.001	1.908E-14	51.0	0.308	17.85	0.191	-5.3	110.4	-71	279
200	0.001	3.645E-14	609.1	0.390	1.82	1.848	63.0	89.6	679	136
240	0.002	7.341E-14	93.0	0.031	1.31	0.047	79.1	14.9	818	35
280	0.004	1.624E-13	102.2	0.016	0.07	0.052	86.7	15.1	880	14
320	0.010	3.783E-13	99.6	0.009	-0.07	0.038	88.3	11.3	893	7
340	0.036	1.360E-12	89.5	0.003	-0.06	0.003	88.6	1.0	895	3
350	0.388	1.477E-11	88.2	0.001	0.00	0.000	88.1	0.1	892	2
360	0.424	1.612E-11	89.6	0.002	-0.03	0.003	88.8	0.9	897	4
380	0.457	1.737E-11	89.4	0.002	0.00	0.004	88.2	1.2	893	2
400	0.610	2.321E-11	88.4	0.001	0.00	0.001	88.1	0.3	892	1
420	0.874	3.323E-11	88.5	0.001	0.00	0.000	88.4	0.1	894	1
430	0.922	3.506E-11	89.0	0.001	-0.01	0.001	88.6	0.4	896	2
440	0.935	3.558E-11	88.8	0.002	-0.04	0.002	88.1	0.7	892	4
560	0.953	3.624E-11	89.7	0.002	-0.04	0.003	88.9	0.9	898	4
700	1.000	3.804E-11	89.5	0.001	0.00	0.001	89.0	0.4	899	2

Table 5. (continued)

Power mW	^{39}Ar fraction	$^{39}Ar_K$ Moles	$^{40}Ar/^{39}Ar$	$^{38}Ar/^{39}Ar$	$^{37}Ar/^{39}Ar$	$^{36}Ar/^{39}Ar$	$^{40}Ar^*/^{39}Ar_K$	% ^{40}Ar Atmos.	Age, Ma	error 1σ, Ma
SRD104 Muscovite (1300 μm)										
40	0.010	1.649E-13	88.4	0.009	0.01	0.012	84.7	4.1	860	11
80	0.024	4.111E-13	91.1	0.008	0.01	0.010	88.1	3.2	887	9
120	0.114	1.925E-12	90.3	0.003	0.00	0.005	88.8	1.6	893	3
130	0.268	4.506E-12	89.5	0.003	0.00	0.001	89.1	0.4	895	1
131	0.342	5.765E-12	89.9	0.003	0.00	0.002	89.2	0.7	896	3
132	0.369	6.219E-12	89.1	0.005	-0.01	0.003	88.3	0.9	889	5
133	0.384	6.457E-12	89.3	0.006	0.00	0.001	88.8	0.4	893	6
140	0.402	6.763E-12	88.9	0.008	-0.01	0.000	88.9	0.1	893	7
160	0.433	7.292E-12	89.9	0.006	0.00	0.002	89.2	0.7	896	4
200	0.791	1.332E-11	88.3	0.003	0.00	0.001	88.0	0.3	886	1
201	0.866	1.458E-11	89.2	0.004	0.00	0.002	88.6	0.6	891	3
220	0.904	1.522E-11	89.8	0.004	0.00	0.002	89.1	0.8	895	5
240	0.932	1.570E-11	90.4	0.006	0.01	0.004	89.1	1.4	895	4
280	0.950	1.599E-11	89.3	0.010	0.00	0.006	87.5	2.0	882	5
360	0.960	1.616E-11	88.7	0.004	0.01	0.003	87.9	0.9	885	9
480	0.984	1.656E-11	88.2	0.006	0.00	0.005	86.7	1.8	875	6
1000	1.000	1.684E-11	89.8	0.007	0.00	0.009	87.0	3.0	878	5

Columns are, from left to right, laser power (beam diameter 1.5 mm); cumulative fraction ^{39}Ar released; moles of K-derived ^{39}Ar in step; isotopic ratios corrected for blank, mass discrimination, Ca-, K-, and Cl-derived Ar isotopic interference, decay of ^{37}Ar, and ^{36}Ar from decay of ^{36}Cl; ratio of radiogenic ^{40}Ar to K-derived ^{39}Ar; % ^{40}Ar atmospheric of total ^{40}Ar in fraction; apparent ages calculated using decay constants recommended by *Steiger and Jäger* [1977]; includes uncertainties in J, mass discrimination, blank, and isotopic measurements. Reported error are 1σ. Grain sizes are measured sizes of grain(s) analyzed. For DHL251 J = 0.00691911 ± 0.00001898, total gas age is 983 ± 2 Ma, plateau age (1764-4000) is 983 ± 1 Ma (mswd = 0.4). For MTG175 J = 0.00722001 ± 0.00000722, total gas age is 1023 ± 1 Ma, plateau age (570-630) is 1014 ± 1 Ma (mswd = 1.2). For RVL20B J = 0.00685122 ± 0.00001532, total gas age is 1029 ± 2 Ma, plateau age (440-2000) is 1034 ± 2 Ma (mswd = 1.0). For BTN195 J = 0.00672999 ± 0.00001237, total gas age is 905 ± 2 Ma, plateau age (500-2000) is 907 ± 1 Ma (mswd = 1.1). For ARN191 J = 0.00726344 ± 0.00000870, total gas age is 910 ± 2 Ma, plateau age (200-600) is 912 ± 2 Ma (mswd = 0.3). For ARN199 J = 0.00722945 ± 0.00000666, total gas age is 924 ± 1 Ma, plateau age (320-372) is 927 ± 1 Ma (mswd = 2.4). For LVT130A J = 0.00725022 ± 0.00000723, total gas age is 893 ± 1 Ma, plateau age (340-420) is 893 ± 1 Ma (mswd = 0.9). For SRD104 J = 0.00720302 ± 0.00000918, total gas age is 890 ± 1 Ma, plateau age (132-360) is 889 ± 1 Ma (mswd = 1.6).

The minimum unroofing rates can be calculated from Figure 5 assuming the rocks were at the surface by circa 590 Ma. The Mazinaw domain was unroofed from 20 km depth between 950 Ma and 590 Ma, yielding an unroofing rate of 0.06 mm/yr. The Sharbot Lake domain was unroofed at rates (averaged from 950 to 590 Ma) that varied from 0.01 mm/yr to 0.03 mm/yr from west to east. These values are minima due to the lack of constraint on the depths of rocks after 900 Ma and 970 Ma for rocks in the footwall and hanging wall, respectively. Although the absolute values of these rates may not be accurate due to lack of constraint on geothermal gradient and low-temperature cooling history, the relative values indicate twice the unroofing rate in the footwall compared to the hanging wall and a three-fold difference in unroofing rate across the Sharbot Lake domain. Given that the RLSZ dips eastward and contains abundant normal shear sense indicators [*Busch and van der Pluijm*, 1995], the differential unroofing between these two domains revealed by different cooling histories supports extensional faulting that juxtaposed higher level rocks of the Sharbot Lake domain (hanging wall) with deeper structural levels in the Mazinaw domain (footwall), which is consistent with greater unroofing rates in the footwall.

The unroofing history indicated by depth calculations at successive times indicates uniform unroofing of the Mazinaw domain. In contrast, the Sharbot Lake domain was unroofed differentially from west to east. Because the unroofing history is based on temperature-time paths, the validity of the associated assumptions must be addressed. If the geothermal gradient varied across the region, the unroofing history may be different than that summarized in Figure 5. For example, if the geothermal gradient were 50°C/km, which is not unreasonable for extensional tectonic settings, the depths calculated would be reduced by ~50%. However, the relative differences of sample depths across the region would still be significant. The 950 Ma depths indicate a structural relief of 15 km across the RLSZ, which would reduce to 7.5 km if the geothermal gradient were 50°C/km in the region. If this apparent structural relief were due to differing geothermal gradients between the hanging wall and footwall, the hanging wall would require a geothermal gradient 1/4 that of the footwall. Similarly, the calculated differential depths across the Sharbot Lake domain could be accounted for by a variation in geothermal gradient within the domain without any depth variation. However, this would require that the geothermal gradient varied by a factor of 2 (25°

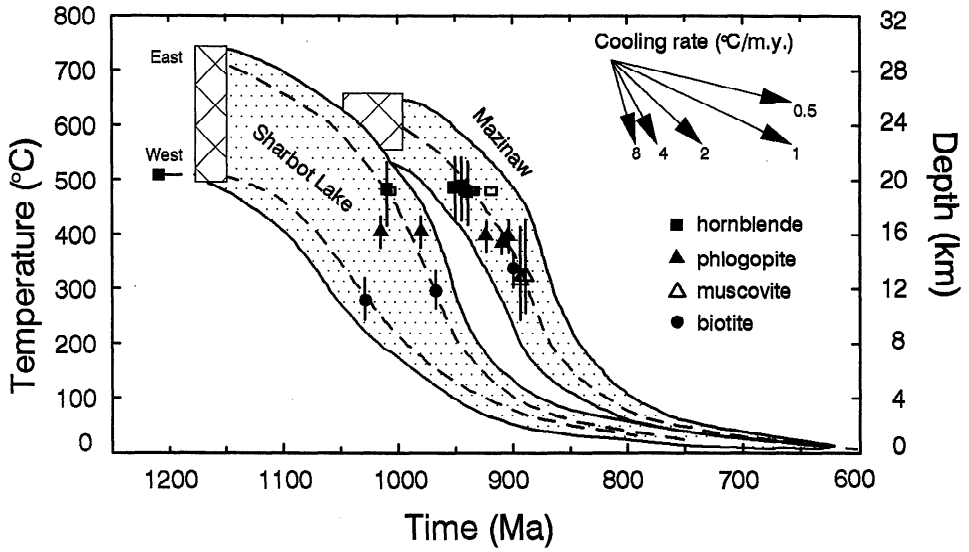

Figure 4. Temperature - time paths for the Mazinaw and Sharbot Lake domains constructed by plotting closure temperature versus cooling age. Error brackets for closure temperatures are the minimum and maximum values calculated from literature data. Errors in cooling ages are less than the symbol size. Data shown with open squares are from *Cosca et al.* [1991, 1992], and biotite ages from *Busch and van der Pluijm* [1995] are included. Cooling rate trajectories are shown in the upper right. The depth scale is determined using a geothermal gradient of 25°C/km. Dashed lines are cooling curves used to extrapolate temperature/depth through time. The different starting temperatures for the two domains correlate with varied peak metamorphic temperatures across the region [*Busch et al.*, (1995)].

to 50°C/km) over a horizontal distance of 15 km, which is unlikely. Thus, although some of the differences in paleodepth may be attributed to perturbed geotherms or uncertainty in closure temperatures, the observed differences are so great that differential unroofing must have occurred.

Structural/Tectonic Implications

Hornblende and mica $^{40}Ar/^{39}Ar$ cooling ages in the Mazinaw domain indicate that the footwall of the RLSZ was at relatively high temperatures (~500°C) at 930-950 Ma and cooled to ~300°C by 900 Ma. This temperature range is consistent with the low temperature mylonitic microstructures observed in the RLSZ [*Busch and van der Pluijm,* 1995]. It is therefore likely that at least some of the mylonites formed during the period from 900 to 950 Ma. Subsequent deformation along the RLSZ is dominated by fracturing, which marks the transition from crystal plastic to brittle deformation [*Busch and van der Pluijm,* 1995]. The transition to frictional deformation processes likely occurred at circa 900 Ma when temperatures reached ~300°C in the footwall and biotite and muscovite closed to Ar diffusion.

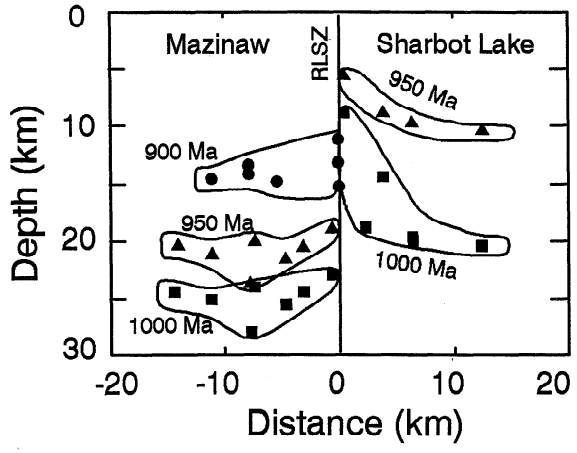

Figure 5. Depth versus distance plot. Distance is measured perpendicular to the strike of the RLSZ. Depths are calculated using the closure temperature (T_c) and a geothermal gradient of 25°C/km (depth = T_c/geothermal gradient). Cooling curves from Figure 4 are used to extrapolate depths through time. Squares are 1000 Ma depths, triangles are 950 Ma depths, and circles are 900 Ma depths.

The distribution in $^{40}Ar/^{39}Ar$ cooling ages across the Mazinaw domain indicates uniform unroofing throughout the domain since 950 Ma (Figures 6a and 6b). Ages in the Sharbot Lake domain (hanging wall) are older toward the shear zone. These data indicate that the hanging wall adjacent to the RLSZ was at shallow depths (12 km) as early as 1029 Ma. Furthermore, the growth age recorded in amphibole in this region indicates that the hanging wall adjacent to the RLSZ was at upper crustal levels since 1205 Ma. In contrast, the eastern Sharbot Lake domain was 20 km deep at 1000 Ma (Figures 5 and 6a). Between 1000 Ma and 590 Ma, rocks in the eastern Sharbot Lake domain have been exhumed from structural levels 10 km deeper than rocks in the western Sharbot Lake domain. A depth differences across the Sharbot Lake domain continued until at least 969 Ma, the youngest cooling age in the domain. The differential exhumation across the Sharbot Lake domain is not accounted for by rotations of the hanging wall (Sharbot Lake domain) until late in the development of this extensional fault system.

Rotations of the hanging wall of fault systems can result from several styles of extension [e.g., *Wernicke and Burchfiel,* 1982]. Domino block faulting on a regional scale could

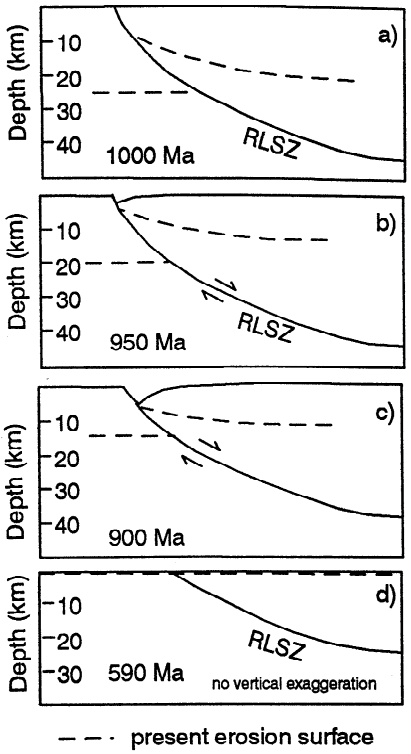

Figure 6. Geometric model explaining the variation in cooling ages across the region. The dashed lines are the present-day erosional surface. (a) At 1000 Ma the Mazinaw domain is in the waning stages of metamorphism, the western Sharbot Lake domain has cooled below 300°C, and central Sharbot Lake domain has cooled below 470°C. (b) At 950 Ma, extension along the RLSZ produces low-temperature mylonites by 900 Ma. (c) The transition to brittle deformation along the RLSZ occurs at circa 900 Ma (300°-350°C) accompanied by differential unroofing. (d) The Proterozoic rocks presently exposed were near the surface by 590 Ma when cut by dikes of the Grenville dike swarm [*Kamo et al.* 1995]. The orientation of the shear zone at depth is taken from *White et al.* [1994].

account for rotations in the hanging wall but does not explain the lack of rotations in the footwall. Displacement on listric normal faults rotates the hanging wall without rotations in the footwall. The RLSZ has been traced to 24 km depth using seismic techniques [*White et al.*, 1994; *Zelt et al.*, 1994]. *Zelt et al.* [1994] concluded from seismic observations that the dip of the shear zone from 8 to 24 km is approximately 13°, which is shallower than the dip of the zone (30°) at its presently exposed level [*Busch and van der Pluijm*, 1995]. The seismic data thus indicate a listric fault geometry that cannot be traced deeper than 24 km and may flatten into a discontinuity currently located at midcrustal levels [*Zelt et al.*, 1994]. The style of late extension of the RLSZ is listric normal faulting whereby the hanging wall adjacent to the RLSZ remained at shallow structural levels due to extensional displacement and the hanging wall away from the RLSZ was unroofed more rapidly (Figure 6). Cooling ages record the magnitude of rotation of the hanging wall (since 1029 Ma) at ~35° (or ~20° using a geothermal gradient of 50°C/km). It is possible that footwall rotations occurred prior to 950 Ma and are not recorded in varied cooling ages in the footwall because the footwall had not cooled below the hornblende closure temperature. A different approach is required to unravel the early extensional history. However, differences in biotite cooling ages across the RLSZ indicate that displacement occurred at least until 900 Ma. Thus the late extensional history of the Grenville orogen is at least locally characterized by listric normal faulting.

Acknowledgments. Grants from the National Science Foundation (EAR 93-05736), the Scott Turner Fund (of the University of Michigan), and Geological Society of America (5122-93) provided financial support for this project. We are grateful for the assistance of Marcus Johnson in the Radiogenic Isotope Geology Laboratory at the University of Michigan. The electron microprobe analyzer used in this work was acquired under Grant EAR 82-12764 from the National Science Foundation. A. Davidson and an anonymous reviewer are thanked for helpful reviews of the manuscript.

References

Baldwin, S.L., T.M. Harrison, and J.D. Fitz Gerald, Diffusion of ^{40}Ar in metamorphic hornblende, *Contrib. Mineral. Petrol., 105*, 691-703, 1990.

Busch, J.P., and B.A. van der Pluijm, Late orogenic, plastic to brittle extension along the Robertson Lake shear zone: Implications for the style of deep-orogenic extension in the Grenville orogen, Canada, *Precambrian Res.*, in press, 1995.

Busch, J.P., E.J. Essene, and B.A. van der Pluijm, Deep crustal normal faulting in the Grenville orogen: Constraints from thermobarometry near the Robertson Lake shear zone, *Tectonophysics*, in press, 1995.

Carmichael, D.M., J.M. Moore, and G.B. Skippen, Isograds around the Hastings Metamorphic "Low", in *Geologial Society of America - Geological Assocociation Canada - Mineralogical Assocociation Canada*, Toronto 1978, Field Trip Guidebook, pp. 325-346, Geological Association of Canada, St. Johns, Newfoundland, 1978.

Carter, T.R., Copper-antimony-gold-silver deposits of the Lavant-Darling area, southeastern Ontario: Geology, genesis and metallogenic significance, M.S. thesis, 203 pp. Univ. of Toronto, Toronto, Ont., Canada, 1981.

Corfu, F., and R.M. Easton, U/Pb geochronology of the Mazinaw terrane, Central Metasedimentary Belt, Grenville Province, Ontario, *Prog. Abstr., Geol. Assoc. Can. Mineral. Assoc. Can. 19*, A22, 1994.

Corfu, F. and R.M. Easton, U/Pb geochronology of the Mazinaw terrane, an imbricate segment of the Central Metasedimentary Belt, Grenville Province, *Can. J. Earth Sci., 32*, 959-976, 1995.

Corfu, F., R.M. Easton, and R.S. Hildebrande, History of Sharbot Lake, Frontenac and Adirondack Lowland terranes, Grenville Province, *Geol. Soc. Am. Prog. Abstr., 27*, A160, 1995.

Cosca, M.A., and R.K. O'Nions, A re-examination of the influence of composition on argon retentivity in metamorphic calcic amphiboles, *Chem. Geol., 112*, 39-56, 1994.

Cosca, M.A., J.F. Sutter, and E.J. Essene, Cooling and inferred uplift/erosion history of the Grenville Orogen, Ontario: Constraints from $^{40}Ar/^{39}Ar$ thermo-chronology, *Tectonics, 10*, 959-977, 1991.

Cosca, M.A., E.J. Essene, M.J. Kunk, and J.F. Sutter, Differential unroofing within the Central Metasedimentary Belt of the Grenville Orogen: Constraints from $^{40}Ar/^{39}Ar$ thermochronology, *Contrib. Mineral. Petrol., 110*, 211-225, 1992.

Cosca, M.A., E.J. Essene, K. Mezger, and B.A. van der Pluijm, Constraints on the duration of tectonic processes: Protracted extension and deep-crustal rotation in the Grenville orogen, *Geology, 23*, 361-364, 1995.

Culshaw, N.G., J.W.F. Ketchum, N. Wodicka, and P. Wallace, Deep crustal extension following thrusting in the southwestern Grenville Province, Ontario, *Can. J. Earth. Sci., 31*, 160-175, 1994.

Cureton, J.S., Late orogenic normal faulting along the Mooroton shear zone, Grenville province, Ontario, Canada, M.S. Thesis, Univ. of Michigan, Ann Arbor, 1994.

Davidson, A., Tectonic boundaries within the

Grenville Province of the Canadian shield, *J. Geodyn., 1*, 433-444, 1984.

Davidson, A., and J.W.F. Ketchum, Observations on the Maberly shear zone, a terrane boundary withing the Central Metasedimentary Belt, Grenville Province, Ontario, in *Current Research Part C., Pap. Geol. Surv. Can., 93-1C*, 265-269, 1993.

Dewey, J.F., Extensional collapse of orogens, *Tectonics, 7*, 1123-1139, 1988.

Dewey, J.F., and K.C.A. Burke, Tibetan, Variscan and Precambrian basement reactivation: Products of continental collision, *J. Geol., 81*, 683-692, 1973.

Dodson, M.H., Closure temperature in cooling geochronological and petrological systems, *Contrib. Mineral. Petrol., 40*, 259-274, 1973.

Dodson, M.H., Theory of cooling ages, in *Lectures in Isotope Geology*, edited by E. Jager and J.C. Hunziker, pp. 195-202, Springer-Verlag, New York, 1979.

Easton, R.M., The Robertson Lake mylonite zone - A major tectonic boundary in the Central Metasedimentary Belt, eastern Ontario, *Prog. Abst. Geol. Assoc. Can. Mineral. Assoc. Can. Can. Soc. Pet. Geol. Joint Meet., 13*, A34-A35, 1988a.

Easton, R.M., *Geology of the Darling area Lanark and Renfrew counties, Open File Rep. Ont. Geol. Surv., 5693*, 206 pp., 1988b.

Easton, R.M., Regional mapping and stratigraphic studies, Grenville Province with some notes on mineralization environments, in *Summary of field work and other activities*, edited by A.C. Colvine et al., *Misc. Pap. Ont. Geol. Surv. 141*, 300-308, 1988c.

Easton, R.M., Part 2, The Grenville Province and the Proterozoic history of central and southern Ontario, in *Geology of Ontario*, edited by P.C. Thurston, H.R. Williams, R.H. Sutcliffe, and G.M. Stott, *Spec. Vol. Ont. Geol. Surv. 4*, 714-904, 1992.

Fillipone, J.A., A. Yin, T.M. Harrison, G. Geherels, M. Smith, and J.C. Sample, Age and magnitude of dip-slip faulting deduced from differential cooing histories: an example from the Hope fault, northwest Montana, *J. Geol., 103*, 199-211, 1995.

Giletti, B.J., Studies in diffusion I: argon in phlogopite mica, in *Geochemical Transport and Kinetics*, edited by A.W. Hofmann, B.J. Giletti, H.S. Yoder Jr., and R.A. Yund, pp. 107-115, Carnegie Institution, Washington, 1974.

Grove, M., and T.M. Harrison, Compositional controls governing argon loss in biotite, *Eos Trans. A. G. U., 74* (16), Spring Meet. Suppl., 339, 1993.

Hames, W.E., and S.A. Bowring, An empirical evaluation of the argon diffusion geometry in muscovite, *Earth Planet. Sci. Lett., 124*, 161-167, 1994.

Hammerschmidt, K., and B. Stöckhert, A K-Ar and $^{40}Ar/^{39}Ar$ study on white micas from the Brixen quartzphyllite, southern Alps, *Contrib. Mineral. Petrol., 95*, 393-406, 1987.

Hanes, J.A., S.J. Clark, and D.A. Archibald, An $^{40}Ar/^{39}Ar$ geochronological study of the Elzevir batholith and its bearing on the tectonothermal history of the southwestern Grenville Province, Canada, *Can J. Earth Sci., 25*, 1834-1845, 1988.

Hanmer, S., Ductile thrusting at mid-crustal levels, southwestern Grenville Province, *Can. J. Earth Sci., 25*, 1049-1059, 1988.

Harrison, T.M., Diffusion of ^{40}Ar in hornblende, *Contrib. Mineral. Petrol., 78*, 324-331, 1981.

Harrison, T.M., and J.D. Fitz Gerald, Exsolution in hornblende and its consequences for $^{40}Ar/^{39}Ar$ age spectra and closure temperature, *Geochim. Cosmochim. Acta, 50*, 247-253, 1986.

Harrison, T.M., and I. McDougall, Investigation of an intrusive contact, northwest Nelson, New Zealand, II, Diffusion of radiogenic and excess ^{40}Ar in hornblende revealed by $^{40}Ar/^{39}Ar$ age spectrum analysis, *Geochim. Cosmochim. Acta, 44*, 2005-2020, 1980.

Harrison, T.M., I. Duncan, and I. McDougall, Diffusion of ^{40}Ar in biotite: Temperature, pressure and compositional effects, Geochim. Cosmochim. Acta, 49, 2461-2468, 1985.

Hutchcon, I., and J.M. Moore, The tremolite isograd near Marble lake, Ontario, *Can. J. Earth Sci., 10*, 936-947, 1973.

Jackson, V.A., Geologic setting of mylonitic rocks in the White Mountain area, Grenville Province, southeastern Ontario, B.S. Thesis, 65 pp. Carlton Univ., Ottawa, Ont., Canada, 1980.

Kamo, S.L., T.E. Krogh, and P.S. Kumarapeli, Age of the Grenville dyke swarm, Ontario - Quebec: Implications for the timing of Iapetan rifting, *Can. J. Earth Sci., 32*, 273-280, 1995.

Leake, B.E., Nomenclature of amphiboles, *Am. Mineral., 63*, 1023-1052, 1978.

Lee, J., Rapid uplift and rotation of mylonitic rocks from beneath a detachment fault: Insights from potassium feldspar $^{40}Ar/^{39}Ar$ thermochronology, northern Snake Range, Nevada, *Tectonics, 14*, 54-77, 1995.

Lumbers, S.B., L.M. Heaman, V.M. Vertolli, and T. Wu, Nature and timing of Middle Proterozoic magmatism in the Central Metasedimentary Belt, Grenville Province, Ontario, in *Mid-Proterozoic Laurentia-Baltica*, edited by C.R. Gower, T. Rivers, and A.B. Ryan, *Spec. Pap. Geol. Assoc. Can., 38*, 243-278, 1990.

McEachern, S.J., and O. van Breemen, Age of deformation within the Central Metasedimentary Belt boundary thrust zone, southwest Grenville Orogen: constraints on the collision of the Mid-Proterozoic Elzevir terrane, *Can. J. Earth Sci., 30*, 1155-1165, 1993.

Meert, J.G., R.B. Hargraves, R. Van der Voo, C.M. Hall, and A.N. Halliday, Paleomagnetic and $^{40}Ar/^{39}Ar$ studies of Late Kibaran intrusives in Burundi, east Africa: Implications for Late Proterozoic supercontinents, *J. Geol., 102*, 621-637, 1994.

Mezger, K., B.A. van der Pluijm, E.J. Essene, and A.N. Halliday, Synorogenic collapse: A perspective from the middle crust, the Proterozoic Grenville Orogen, *Science, 254*, 695-698, 1991.

Mezger, K., E.J. Essene, B.A. van der Pluijm, and A.N. Halliday, U-Pb geochronology of the Grenville Orogen of Ontario and New York: Constraints on ancient crustal tectonics, *Contrib. Mineral. Petrol., 114*, 13-26, 1993.

O'Nions, R.K., D.G.W. Smith, H. Baadsgaard, and R.S. Morton, Influence of chemical composition on argon retentivity in metamorphic calcic amphiboles from south Norway, *Earth Planet. Sci. Lett., 5*, 339-345, 1969.

Pauk, L., *Geology of the Lavant area, Lanark and Frontenac Counties, Rep. Ont. Geol. Surv., 253*, 61 pp., 1989a.

Pauk, L., *Geology of the Dalhousie Lake area, Lanark and Frontenac Counties, Rep. Ont. Geol. Surv., 245*, 57 pp., 1989b.

Platt, J.P., and P.C. England, Convective removal of lithosphere beneath mountain belts: Thermal and mechanical consequences, *Am. J. Sci., 293*, 307-336, 1994.

Pouchou, J.L., and F. Pichoir, A new model for quantitative X-ray microanalysis, I, Application to the analysis of homogeneous samples, *Rech. Aérosp., 3*, 13-38, 1984.

Rivers, T., J. Martignole, C.F. Gower, and A. Davidson, New tectonic subdivisions of the Grenville Province, Southeast Canadian Shield, *Tectonics, 8*, 63-84, 1989.

Sager-Kinsman, E.A., and R.R. Parrish, Geochronology of detrital zircons from the Elzevir and Frontenac terranes, Central Metasedimentary Belt, Grenville Province, Ontario, *Can. J. Earth Sci., 30*, 465-473, 1993.

Samson, S.D., and E.C. Alexander Jr., Calibration of the interlaboratory ^{40}Ar-^{39}Ar dating standard, MMhb-1, *Chem. Geol., 66*, 27-34, 1987.

Sethuraman, K., and J.M. Moore, Petrology of metavolcanic rocks in the Bishop Corners - Donaldson Area, Grenville Province, Ontario, *Can. J. Earth Sci., 10*, 589-614, 1973.

Smith, B.L., Geology of the Clarendon-Dalhousie area, *Ont. Dep. Mines Annu. Rep. 1956, 45*, 1-46, 1958.

Snee, L.W., J.F. Sutter, and W.C. Kelly, Thermochronology of economic mineral deposits: Dating the stages of mineralization at Panasqueira, Portugal, by high-precision $^{40}Ar/^{39}Ar$ age spectrum techniques on muscovite, *Econ. Geol., 83*, 335-354, 1988.

Steiger, R.H., and E. Jäger, Subcommission on geochronology: Convention on the use of decay constants in geo- and cosmochronology, *Earth Planet. Sci. Lett., 36*, 359-362, 1977.

van Breemen, O., and A. Davidson, U-Pb zircon ages of granites and syenites in the Central Metasedimentary Belt, Grenville Province, Ontario: Radiogenic age and isotopic studies, Report 2, *Pap. Geol. Surv. Can., 88-2*, 45-50, 1988.

van der Pluijm, B.A., and K.A. Carlson, Extension in the Central Metasedimentary Belt of the Ontario Grenville: Timing and tectonic significance, *Geology, 17*, 161-164, 1989.

van der Pluijm, B.A., K. Mezger, M.A. Cosca, and E.J. Essene, Determining the significance of high-grade shear zones by using temperature-time paths, with examples from the Grenville orogen, *Geology, 22*, 743-746, 1994.

Wallach, J.L., Origin of the Hinchinbrooke gneiss and its age relationship to Grenville Group rocks of southeastern Ontario, paper presented at the Geological Association of Canada Annual Meeting, Geol. Assoc. of Can., St. Johns Newfoundland, 1974.

Wernicke, B., and B.C. Burchfiel, Modes of extensional tectonics, *J. Struct. Geol., 4*, 105-115, 1982.

White, D.J., R.M. Easton, N.G. Culshaw, B. Milkereit, D.A. Forsyth, S. Carr, A.G. Green, and A. Davidson, Seismic images of the Grenville Orogen in Ontario, *Can. J. Earth Sci., 31*, 293-307, 1994.

Windley, B.F., Comparative tectonics of the western Grenville and the western Himalaya, in The Grenville Province, edited by J.M. Moore, A. Davidson and A.J. Baer, *Spec. Pap. Geol. Assoc. Can., 31*, 341-348, 1986.

Wolff, J.M., *Geology of the Sharbot Lake area, Frontenac and Lanark counties southeastern Ontario, Rep. Ont. Geol. Surv. 228*, 70 pp., 1985.

Zelt, C.A., D.A. Forsyth, B. Milkereit, D.J. White, I. Asudeh, and R.M. Easton, Seismic structure of the Central Metasedimentary Belt, southern Grenville Province, *Can. J. Earth Sci., 31*, 243-254, 1994.

J. P. Busch, E. J. Essene, C. M. Hall, and B. A. van der Pluijm, Department of Geological Sciences, University of Michigan, 2534 C.C. Little Bldg., Ann Arbor, MI 48109-1063 (e-mail: jaybusch@umich.edu; essene@umich.edu; cmhall@umich.edu; vdpluijm@umich.edu)

(Received October 26, 1995;
accepted November 1, 1995)